materials

MDPI

Article

Magnetic Anisotropy and Damping Constant of Ferrimagnetic GdCo Alloy near Compensation Point

Sungjung Joo [1], Rekikua Sahilu Alemayehu [2], Jong-Guk Choi [3], Byong-Guk Park [3] and Gyung-Min Choi [2,4,*]

[1] Center for Electromagnetic Metrology, KRISS, Daejeon 34113, Korea; joosj@kriss.re.kr
[2] Department of Energy Science, Sungkyunkwan University, Suwon 16419, Korea; rekiks2@gmail.com
[3] Department of Materials Science and Engineering, KAIST, Daejeon 34141, Korea; cjg000@kaist.ac.kr (J.-G.C.); bgpark@kaist.ac.kr (B.-G.P.)
[4] Center for Integrated Nanostructure Physics, Institute for Basic Science (IBS), Suwon 16419, Korea
* Correspondence: gmchoi@skku.edu; Tel.:+82-31-299-6279

Abstract: Metallic ferrimagnets with rare earth-transition metal alloys can provide novel properties that cannot be obtained using conventional ferromagnets. Recently, the compensation point of ferrimagnets, where the net magnetization or net angular momentum vanishes, has been considered a key aspect for memory device applications. For such applications, the magnetic anisotropy energy and damping constant are crucial. In this study, we investigate the magnetic anisotropy and damping constant of a GdCo alloy, with a Gd concentration of 12–27%. By analyzing the equilibrium tilting of magnetization as a function of the applied magnetic field, we estimate the uniaxial anisotropy to be 1–3 $\times$ 10^4 J m^{-3}. By analyzing the transient dynamics of magnetization as a function of time, we estimate the damping constant to be 0.08–0.22.

Keywords: ferrimagnet; GdCo alloy; magnetic anisotropy; damping constant

Citation: Joo, S.; Alemayehu, R.S.; Choi, J.-G.; Park, B.-G.; Choi, G.-M. Magnetic Anisotropy and Damping Constant of Ferrimagnetic GdCo Alloy near Compensation Point. *Materials* **2021**, *14*, 2604. https://doi.org/10.3390/ma14102604

Academic Editors: Voicu Octavian Dolocan and Sylvain Bertaina

Received: 20 April 2021
Accepted: 14 May 2021
Published: 17 May 2021

1. Introduction

Rare earth (RE)-transition metal (TM) alloys can have a ferrimagnetic phase, where the magnetizations of the RE and TM sublattices have antiparallel alignment. RE-TM ferrimagnets possess many interesting properties; e.g., perpendicular magnetic anisotropy without long-range crystalline ordering [1–4], all-optical switching of magnetization [5,6], net magnetization vanishing at the compensation point [7,8]. Recently, RE-TM ferrimagnets have been considered as information-storage elements for memory devices of magnetic-random access memory and race track memory [9–15]. An advantage of RE-TM ferrimagnets over conventional TM ferromagnets in terms of operation speed and power consumption has been demonstrated near the compensation point, where the magnetization or angular momentum of RE and TM cancel each other out. To gain more insights into the application of RE-TM ferrimagnets to memory devices, additional information regarding magnetic anisotropy and damping is required. The magnetic anisotropy determines the thermal stability of the memory element, and the damping constant determines the switching current in the writing process [16–18].

In this study, we investigate the magnetic anisotropy and damping of a GdCo alloy, with a Gd concentration of 12–27%. The GdCo alloy is a common material that has been used for memory devices owing to its ability to tune the net magnetization and perpendicular magnetic anisotropy. To investigate magnetic anisotropy, we measure the out-of-plane magnetization as a function of the in-plane magnetic field. Analyzing the equilibrium tilting of the magnetization, we determine the uniaxial magnetic anisotropy of 2.8 $\times$ 10^4 J m^{-3} at the compensation point. To investigate damping, we measure the transient dynamics of magnetization, triggered by sudden change of anisotropy energy. Analyzing the relaxation of the magnetization precession, we determine the enhanced damping of 0.22 at the compensation point.

2. Materials and Methods

We fabricate samples of Ta (3)/Pt (5)/GdCo (10)/Ta (3) structures using magnetron sputtering on thermally oxidized silicon substrates; the numbers in the parentheses are in nm. The Ta/Pt layer acts as an underlayer of the GdCo alloy. Although the GdCo alloy has an amorphous structure without a structural phase, the underlayer affects the magnetic anisotropy of the GdCo alloy. We find that the GdCo alloy with the Ta/Pt underlayer provides a larger magnetic anisotropy than without underlayer. The exact mechanism is not known, but experimental observation of the underlayer effect has been reported with amorphous ferrimagnets of GdTbCo and TbFeCo alloys [19,20]. In this work, we fix the underlayer and vary the Gd concentration from 12% to 27% of the GdCo layer. The GdCo composition is adjusted by controlling the sputter power of the Gd and Co targets during co-sputtering. Since the deposition rate of each target is approximately proportional to the sputter power, we can control the flux of Gd and Co atoms on the substrate during the deposition. The actual composition of the GdCo film was check by Energy–dispersive X-ray Spectroscopy. The top Ta layer acts as a capping layer to protect the GdCo layer from oxidation. Regarding sputtering conditions, we use the Ar pressure of 3 mTorr, target–to–substrate distance of 200 mm, and deposition rate of 0.06–0.12 nm s^{-1}. The deposition rate of each layer is predetermined with a single thick layer, whose thickness is determined by X-ray reflectivity measurements, then the thickness of each layer is controlled by deposition time. All layers are deposited at room temperature.

We investigate magnetic anisotropy using the generalized Sucksmith-Tompson (GST) method [21–23]. The GST method analyzes the out-of-plane magnetization in an oblique magnetic field, a combination of the in-plane field to tilt magnetization and the out-of-plane field to maintain a single domain. To accurately quantify the out-of-plane magnetization, we use a vibrating sample magnetometer (VSM) and the anomalous Hall effect (AHE). The VSM measures the stray field from magnetization and enables quantification of the absolute magnitude of magnetization. The AHE measures the anomalous voltage (V_{AHE}) in the presence of the charge current (I_{c}) and magnetization (M) as $\vec{V}_{\mathrm{AHE}} \propto \vec{I}_{\mathrm{c}} \times \vec{M}$ [24]. When I_{c} and M are along the x and z directions, respectively, V_{AHE} is along the y direction. Because the AHE originates from the electrons near the Fermi level, it does not provide the absolute magnitude of magnetization but accurately measures the relative magnitude of the out-of-plane magnetization, $m_z = M_z/|M|$, because of the large signal-to-noise ratio of V_{AHE}. We connect wire bonding at the four corners of the square-shaped sample, size of 1.27×12.7 cm^2, to measure V_{AHE} in the van der Pauw geometry. We measure V_{AHE}, with a DC charge current of 1 mA, as a function of the magnetic field with an oblique angle in the z-direction.

We investigate damping constants using time-resolved magneto-optical Kerr effect (TRMOKE). The TRMOKE is based on an optical pump-probe technique; i.e., a pump pulse excites the sample, and a probe pulse measures the response of the sample with a controlled time delay between the pump and probe. When a pump pulse causes a sudden change in the magnetic anisotropy, a precessional motion of the magnetization occurs [25]. A probe pulse measures the magnetization dynamics via MOKE. We use a polar MOKE geometry, so that the probe pulse measures the z component of the magnetization. We use a Ti-sapphire femtosecond laser to produce the pump and probe pulses. The wavelengths of the pump and probe are 784 nm. The pulse widths are 1.1 ps for the pump and 0.2 ps for the probe. (The pump pulse is elongated by a group velocity dispersion of the electro-optic modulator.) To increase the signal-to-noise ratio, we modulate the pump and probe plus at a frequency of 10 MHz and 200 Hz, respectively, using an electro-optic modulator and optical chopper. Both pump and probe beams are focused on the sample surface, which is covered by a 3 nm Ta capping layer, with a spot size of 6 μm. The Kerr rotation of the reflected probe beam is measured by a combination of the Wollaston prism and a balanced photodetector.

3. Results

3.1. Basic Magnetic Properties

As basic magnetic properties, we measure the hysteresis of magnetization of the GdCo alloy by applying a magnetic field along the out-of-plane and in-plane directions (Figure 1). At Gd concentrations of 18–27%, the GdCo alloy has a perpendicular magnetic anisotropy, whereas it has an in-plane magnetic anisotropy at Gd concentration of 12–15%. In particular, the net magnetization critically depends on the Gd concentration, and it becomes minimum at a Gd concentration of 24%. Therefore, Gd = 24% is close to the magnetic compensation point. In addition, the coercivity field of the perpendicularly magnetized GdCo alloy reaches a maximum at a Gd concentration of 24%. The coercivity field is often proportional to the perpendicular magnetic anisotropy; accordingly, one may expect the divergence of the magnetic anisotropy at the compensation point. However, a vanishing magnetization compensates for the divergence of the coercivity field. The saturation field along the hard axis can be used for a rough estimation of the magnetic anisotropy energy. Unfortunately, the saturation field is beyond the maximum field of VSM, and the VSM signal becomes too weak with a vanishing net magnetization near the compensation point.

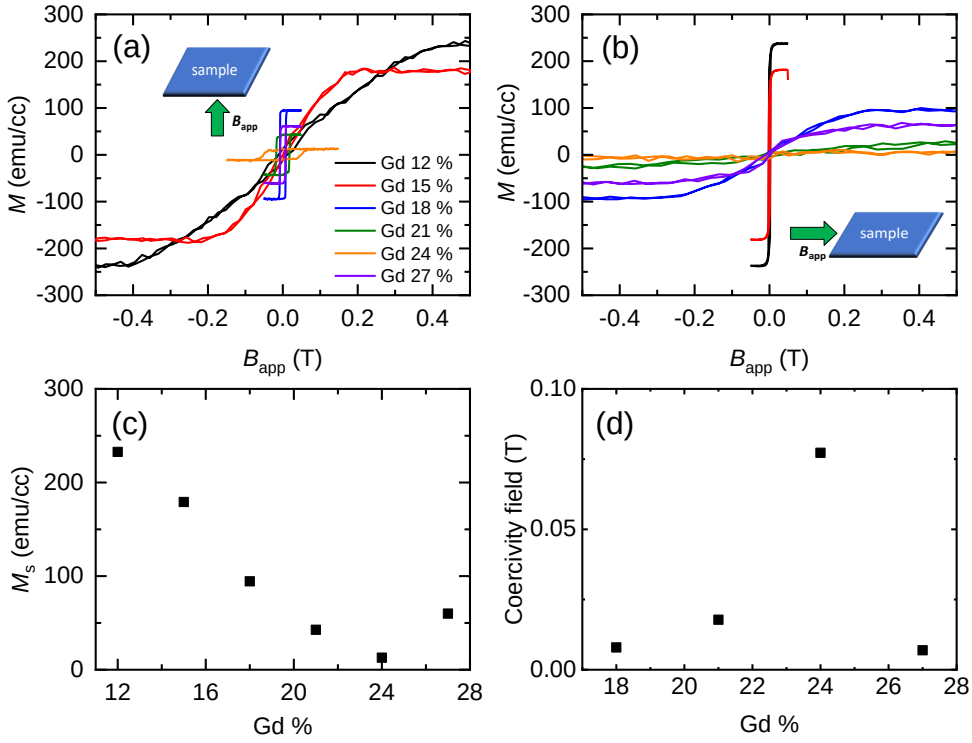

Figure 1. VSM results. Magnetization hysteresis of the Gd_xCo_{1-x} alloy, x from 12% to 27%, applying the magnetic field (**a**) out-of-plane and (**b**) in-plane directions. (**c**) The saturation magnetization of the Gd_xCo_{1-x} alloy. (**d**) The coercivity field of the out-of-plane anisotropy Gd_xCo_{1-x} alloy.

3.2. Determination of Magnetic Anisotropy

To determine the uniaxial magnetic anisotropy of the GdCo alloy, we apply the GST method to the AHE reading of the normalized out-of-plane magnetization, $m_z = \cos\theta_M$, where θ_M is the angle of magnetization from the sample normal (Figure 2). The AHE reading is advantageous over VSM reading in terms of signal-to-noise ratio. As the GST method analyze many m_z data with different applied fields (B_{app}), it is more accurate than the analysis based on one data point at the saturation field. In addition, as the GST method analyze the gradual change in m_z with respect to B_{app}, its field requirement is smaller than the saturation field.

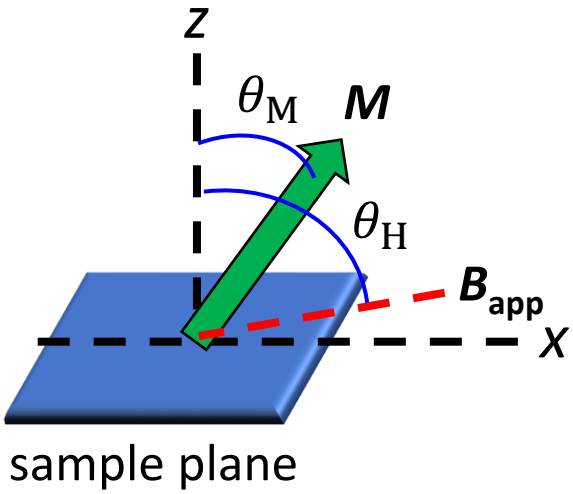

Figure 2. Angle definition for AHE measurements. The normal to the sample plane is defined as the z axis. When a magnetic field (B_{app}) is applied at the angle of θ_H with respect to the z axis, the magnetization (M) tilts at an angle of θ_M, which is determined by the balance between the uniaxial anisotropy energy and Zeeman energy.

We measure m_z using AHE with applying B_{app} at an oblique angle of θ_H = 0° or 85° (Figure 2). At θ_H of 0°, m_z is nearly independent of B_{app} because AHE signal, which is linearly proportional to M, dominates the ordinal Hall signal, which is linearly proportional to B_{app}. With a large θ_H of 85°, m_z gradually decreases with B_{app} as the in-plane component of B_{app} tilts the magnetization (Figure 3). (θ_H should be less than 90° to have an out-of-plane component of B_{app}, which suppresses multidomain formation.) According to the GST method, the relationship between m_z and B_{app} can be expressed as [22],

$$2\left(K_1 - \frac{\mu_0}{2}M_S^2\right) + 4K_2\left(1 - m_z^2\right) = FB_{app}M_S, \quad (1)$$

where K_1 and K_2 are the first and second-order uniaxial anisotropies, M_S is the saturation magnetization of the GdCo alloy, and F is given by

$$F = \frac{m\sin\theta_H - \sqrt{1-m_z^2}\cos\theta_H}{m_z\sqrt{1-m_z^2}}. \quad (2)$$

Plotting $FB_{app}M_S$ vs. $1 - m_z^2$, K_1 and K_2 can be determined independently of the intercept and slope, respectively (Figure 3). (For the Gd = 24%, the measured range of the $1 - m_z^2$ is small because the maximum B_{app} of 1.7 T is much smaller than the saturation field of $B_{sat} \approx \frac{2K_{tot}}{M_S}$, where K_{tot} is the total anisotropy.) The determined values of K_1 and K_2 with Gd concentrations of 18%, 21%, 24%, and 27% are summarized in Table 1. The maximum $K_{tot} = K_1 + K_2$ of 2.8 × 10^4 J m^{-3} is obtained at the compensation point of Gd = 24%. Previously reported values of K_{tot} of the GdCo alloy are in the range of 10^4 J m^{-3}, depending on the Gd concentration and deposition method [1,2,20]. We note that the anisotropy energy of the GdCo alloy is about two orders of magnitude smaller than that of FePt, a well-known ferromagnet for strong magnetic anisotropy [22,23]. Such a low magnetic anisotropy of the GdCo alloy limits the application to memory devices. Interestingly, K_2 becomes larger than K_1 at the compensation point. This observation is surprising because K_1 is usually much larger than K_2 for typical ferromagnets [22,23]. To understand the physical origin for the strong enhancement of K_2 at the compensation point, further theoretical and experimental works are required.

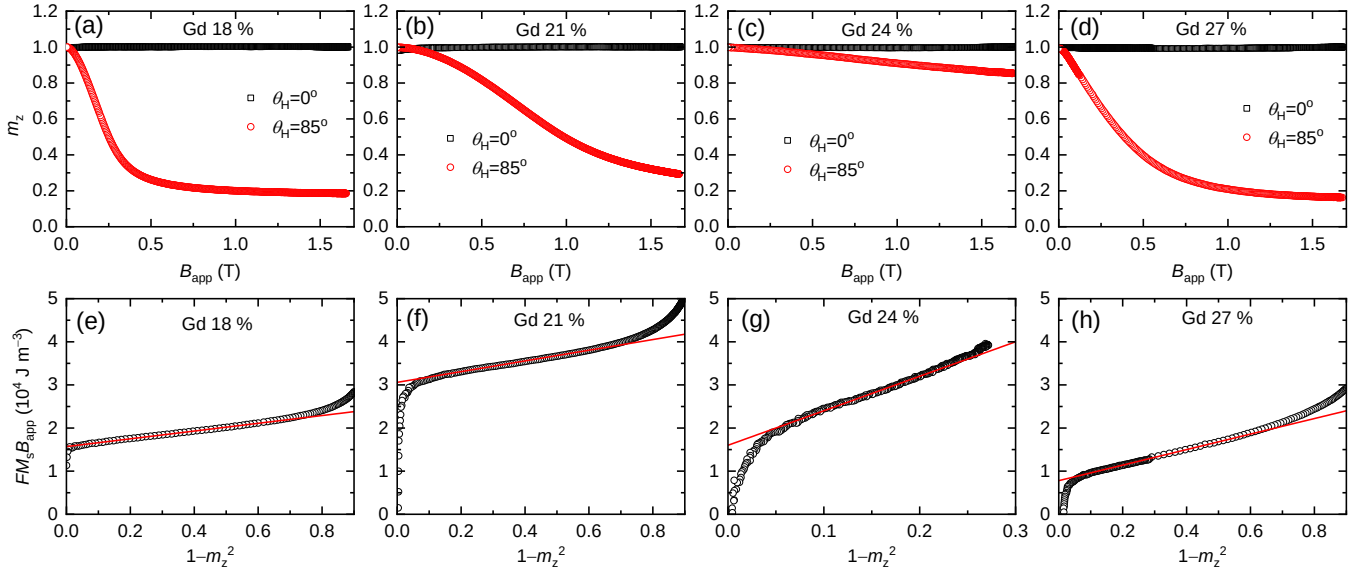

Figure 3. AHE results. The normalized AHE voltage (m_z) of the (**a**) $Gd_{18}Co_{82}$, (**b**) $Gd_{21}Co_{79}$, (**c**) $Gd_{24}Co_{76}$, and (**d**) $Gd_{27}Co_{73}$ alloys. The magnetic field is applied with an oblique angle, θ_H, with respect to the film normal direction. The black/red color corresponds to the θ_H of 0°/85°. The GST analysis of the (**e**) $Gd_{18}Co_{82}$, (**f**) $Gd_{21}Co_{79}$, (**g**) $Gd_{24}Co_{76}$, and (**h**) $Gd_{27}Co_{73}$ alloys. The black squares are the data obtained from (**a**–**d**) with θ_H of 85°. The red lines are fittings with Equation (1). The fitted values of the uniaxial anisotropy are summarized in Table 1.

Table 1. The first-order (K_1) and second-order (K_2) uniaxial anisotropy of the GdCo alloy, with the Gd concentration of 18%, 21%, 24%, and 27%. The $K_1{}^{eff}$ and K_2 values are determined from the linear fitting of Figure 2e–h. The K_1 values are obtained from $K_1{}^{eff}$ by $K_1 = K_1{}^{eff} + \mu_0 M^2/2$.

Colume Heading	$Gd_{18}Co_{82}$	$Gd_{21}Co_{79}$	$Gd_{24}Co_{76}$	$Gd_{27}Co_{73}$
$K_1{}^{eff}$ (J m^{-3})	7.9×10^3	15.3×10^3	8×10^3	3.9×10^3
$\mu_0 M^2/2$ (J m^{-3})	5.6×10^3	1.1×10^3	0.1×10^3	2.3×10^3
K_1 (J m^{-3})	13.5×10^3	16.4×10^3	8.1×10^3	6.2×10^3
K_2 (J m^{-3})	2.3×10^3	3.1×10^3	20×10^3	4.5×10^3
$K_1 + K_2$ (J m^{-3})	15.8×10^3	19.5×10^3	28.1×10^3	10.7×10^3

3.3. Determination of Damping Constant

To determine damping constants of the GdCo alloy, we measure the magnetization dynamics using TRMOKE. We use four samples with Gd concentrations of 12%, 18%, 24%, and 27%. The Gd = 12% has in-plane anisotropy, whereas others have out-of-plane anisotropy. To trigger the magnetization precession, we need to apply B_{app} along the z/x direction for the in-plane/out-of-plane anisotropy sample. We apply a B_{app} of 0.3 T along the x direction for the $Gd_{18}Co_{82}$, $Gd_{24}Co_{76}$, and $Gd_{27}Co_{73}$ samples and B_{app} of 0.5 T along the z direction for the $Gd_{12}Co_{88}$ sample. The magnitude of B_{app} is chosen to be larger than the saturation field along the hard axis, so that the initial magnetization aligns along the x or z direction (Figure 1). (This is not the case for the Gd = 24%, in which the saturation field is much larger than B_{app} of 0.3 T.) Such an alignment makes the damping analysis to be simple. The equilibrium direction of magnetization is determined by the balance between the uniaxial anisotropy, demagnetization field, and external field. When a pump pulse induces an ultrafast demagnetization via sudden heating, the balance is suddenly disturbed, and a precessional motion of magnetization is triggered [25]. Indeed, the TRMOKE shows a precessional motion on top of an ultrafast demagnetization (Figure 4). We separate the precessional motion by subtracting the demagnetization background signal from the raw data. The precessional motion can be described by the Landau–Lifshitz–Gilbert equation based on the mean-field model [26–29],

$$\frac{\mathrm{d}}{\mathrm{d}t}\vec{M}_{\mathrm{eff}} = -\gamma_{\mathrm{eff}}\vec{M}_{\mathrm{eff}} \times \vec{H}_{\mathrm{eff}} + \frac{\alpha_{\mathrm{eff}}}{M_{\mathrm{eff}}}\left(\vec{M}_{\mathrm{eff}} \times \frac{\mathrm{d}}{\mathrm{d}t}\vec{M}_{\mathrm{eff}}\right), \quad (3)$$

where M_{eff} is the net magnetization of the GdCo alloy, γ_{eff} is the effective gyromagnetic ratio of the GdCo alloy, H_{eff} is the effective field combining the exchange field, anisotropy field, demagnetization field, and external field, and α_{eff} is the effective damping of the GdCo alloy. Alternatively, α_{eff} can be obtained as $\alpha_{\mathrm{eff}} = 1/(2\pi f\tau)$, where f is the precession frequency, and τ is the relaxation time of the damped cosine function of $\cos(2\pi ft) \times \exp(-t/\tau)$.

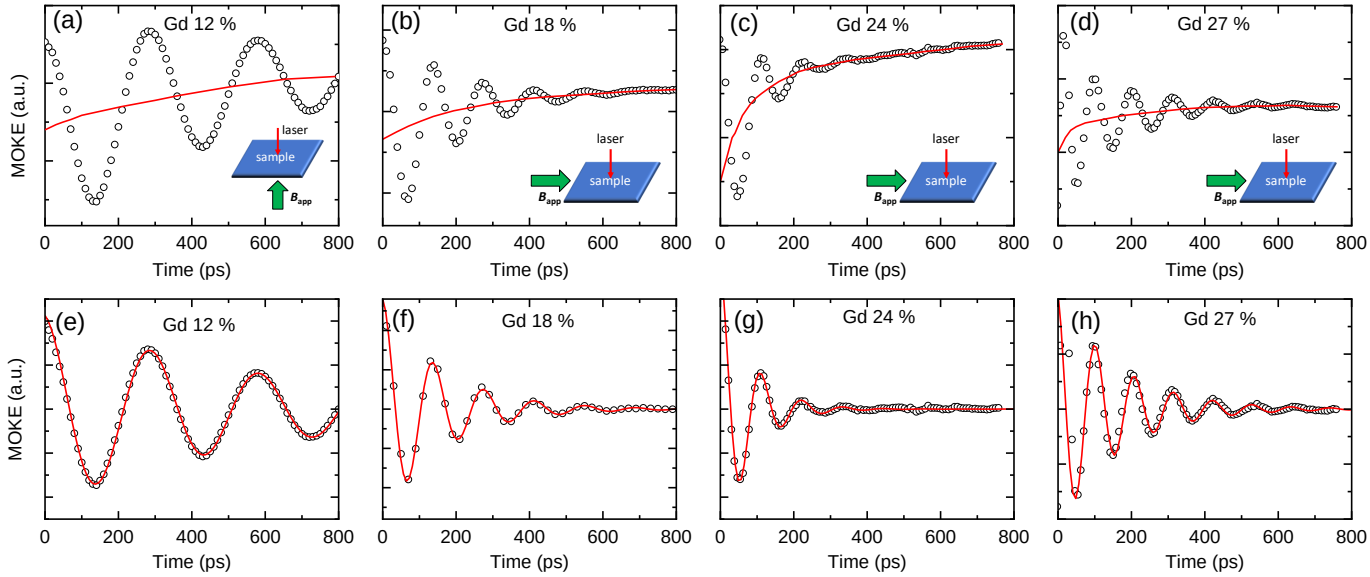

Figure 4. TRMOKE results. The magnetization dynamics triggered by a pump pulse in the (**a**) $Gd_{12}Co_{88}$, (**b**) $Gd_{18}Co_{72}$, (**c**) $Gd_{24}Co_{76}$, and (d) $Gd_{27}Co_{73}$ alloys. A magnetic field of 0.5 T/0.3 T is applied along the z/x direction for (**a**)/(**b**–**d**). The black circles are the measure data. The red lines are the background demagnetization signal. The extracted precessional motion in the (**e**) $Gd_{12}Co_{88}$, (**f**) $Gd_{18}Co_{72}$, (**g**) $Gd_{24}Co_{76}$, and (**h**) $Gd_{27}Co_{73}$ alloys. The black circles are obtained by subtracting the demagnetization background from the raw data of (**a**–**d**). The red lines are fittings by damped cosine function of $\cos(2\pi ft) \times \exp(-t/\tau)$. The fitted f values are 3.4, 7.2, 8.9, and 9.4 GHz for (**e**–**h**), respectively. The fitted τ values are 600, 160, 80, and 160 ps for (**e**–**h**), respectively.

We summarize the determined values of K_{tot} (K_1 + K_2) and α_{eff} in Figure 5. Both K_{tot} and α_{eff} maximize at the compensation point of Gd = 24%. Here, α_{eff} is not the intrinsic parameter, but depends on B_{app}. For the $Gd_{18}Co_{82}$ and $Gd_{27}Co_{73}$ alloys, when magnetization aligns nearly to the x direction by B_{app}, the intrinsic damping (α_{int}) is related to α_{eff} as [30],

$$\alpha_{\mathrm{int}} \approx \alpha_{\mathrm{eff}}\frac{2\sqrt{B_1 B_2}}{B_1 + B_2}, \quad (4)$$

where $B_1 = B_{\mathrm{app}} + B_{\mathrm{K}}$, $B_2 = B_{\mathrm{app}}$, and $B_{\mathrm{K}} = (2K_1 - \mu_0 M_{\mathrm{S}} + 4K_2)/M_{\mathrm{S}}$. For the $Gd_{24}Co_{76}$ alloy, magnetization aligns nearly to the z direction by strong B_{ani}, then $\alpha_{\mathrm{int}} \approx \alpha_{\mathrm{eff}}$. The variation of α_{eff} of the $Gd_{24}Co_{76}$ alloy with different B_{app} is shown in Appendix A. Using the B_{K} information in Table 1, we show that α_{int} also maximize at Gd = 24% with a peak value of 0.22. Our result of α = 0.22 is consistent with previous reports of 0.2–0.3 of the GdCo and GdFeCo alloys from the ferromagnetic resonance and TRMOKE measurements [26–28]. However, much low α of 0.007 of the GdFeCo alloy was reported from the measurement of the domain wall motion [31]. Further studies are required to resolve this discrepancy between measurement techniques.

Note that the pump pulse induces a significant temperature rise in the sample. Considering $\Delta T \approx F_{\mathrm{in}} A_{\mathrm{tot}}/C_{\mathrm{V}} d_{\mathrm{tot}}$, where F_{in} is the incident fluence of the pump of 12 J m^{-2}, A_{tot} is the absorption coefficient by the total metal layers of $\approx$ 0.3, C_{V} is the typical heat capacity of metals of 3 $\times$ 10^6 J m^{-3} K^{-1}, and d_{tot} is the total thickness of metal layers of 21 nm,

the temperature rise of the sample would be approximately 60 K (ignoring the slow heat transfer to the substrate). Because the alloy concentration for the magnetic compensation depends on temperature, the $Gd_{24}Co_{76}$ alloy may not be the magnetic compensation point during TRMOKE. We claim that the increase in α_{eff} is caused by the angular momentum compensation between the Gd and Co sublattices. Such enhancement of α_{eff} near the compensation point has been previously reported for the GdFeCo and GdCo alloys, and the mean-field model was used to explain the physical origin [26–28]. According to the mean-field model, α_{eff} of the GdCo alloy is expressed as [29],

$$\alpha_{eff} = \frac{\alpha_{Co} M_{Co}/\gamma_{Co} + \alpha_{Gd} M_{Gd}/\gamma_{Co}}{M_{Co}/\gamma_{Co} - M_{Gd}/\gamma_{Co}}, \quad (5)$$

where α_{Co}/α_{Gd} is the damping constant of the Co/Gd sublattice, M_{Co}/M_{Gd} is the magnetization of the Co/Gd sublattice, and γ_{Co}/γ_{Gd} is the gyromagnetic ratio of the Co/Gd sublattice. Accordingly, α_{eff} diverges at the compensation of the angular momentum, M/γ. Typically, the angular momentum compensation temperature is 50–100 K higher than the magnetization compensation temperature [13,15,27].

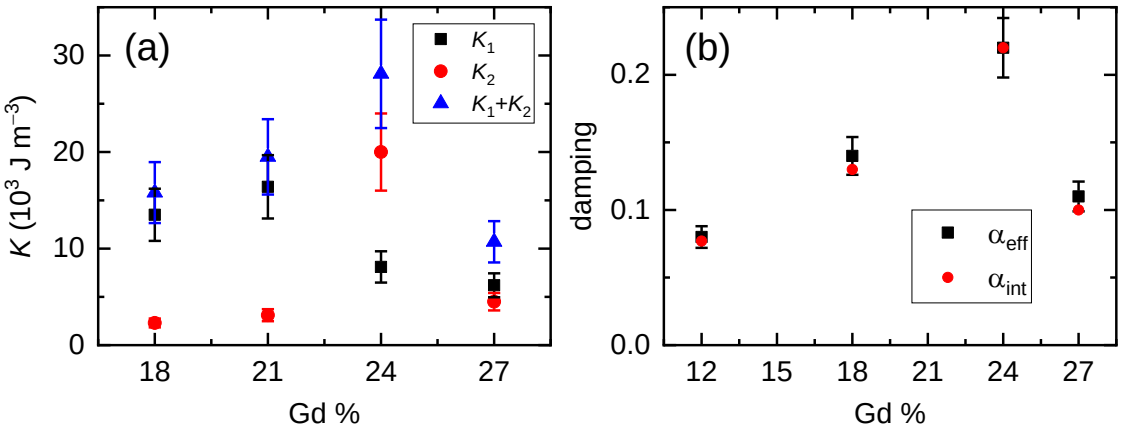

Figure 5. Summary of the uniaxial anisotropy (K) and damping constant (α). (**a**) The K values of the GdCo alloy. The black square/red circle/blue triangle corresponds to the first order (K_1)/second order (K_2)/total (K_1 + K_2) anisotropy. The error range in the K_1 and K_2 determination is 20% considering the 10% uncertainty in M_S of VSM measurements and $\pm 1°$ error in θ_H of AHE measurements. (**b**) The α values of the GdCo alloy. The black square/red circle corresponds to the effective damping (α_{eff})/intrinsic damping (α_{int}). The α_{eff} is obtained from the fitting of the precession motion. The α_{int} is obtained using Equation (4) for the Gd = 12%, 18%, and 27%. For the Gd = 24%, we assume α_{int} is the same as α_{eff}. The error range in the α_{eff} determination is 10% considering the fitting uncertainties of f and τ.

4. Discussion

We investigate the magnetic anisotropy energy and damping constant of the GdCo alloy. By applying the GST method to the AHE measurements, we determine the uniaxial anisotropy energy of 2.8×10^4 J m^{-3} at the compensation point, Gd concentration of 24%. Surprisingly, we find that the second-order uniaxial anisotropy becomes larger than the first-order one at the compensation point. We expect that this anisotropy inversion is related to the magnetization compensation. Measuring the magnetization dynamics using TRMOKE, we determine the damping constant. An enhanced damping constant of 0.22 is observed at the compensation point. This enhancement is consistent with previous reports and can be understood by the angular momentum compensation.

Author Contributions: Conceptualization, B.-G.P. and G.-M.C.; Sample preparation: J.-G.C. and B.-G.P.; VSM investigation: J.-G.C. and B.-G.P.; AHE investigation, S.J.; TRMOKE investigation: R.S.A. and G.-M.C.; writing—original draft preparation, G.-M.C. All authors have read and agreed to the published version of the manuscript.

Funding: G.-M.C. is funded by the National Research Foundation of Korea (2019R1C1C1009199, 2018M3D1A1058793). B.-G.P. is funded by the National Research Foundation of Korea (2020R1A2C2010309).

Institutional Review Board Statement: Not applicable.

Informed Consent Statement: Not applicable.

Data Availability Statement: Derived data supporting the findings of this study are available from the corresponding author (G.-M.C.) on request.

Conflicts of Interest: The authors declare no conflict of interest.

Appendix A

We measure the magnetization precession of the $Gd_{24}Co_{76}$ alloy with three different B_{app} of 0.2, 0.3, and 0.4 T. From the fittings with a damped cosine function, we determine the same α_{eff} of 0.22 $\pm$ 0.02 for all three conditions.

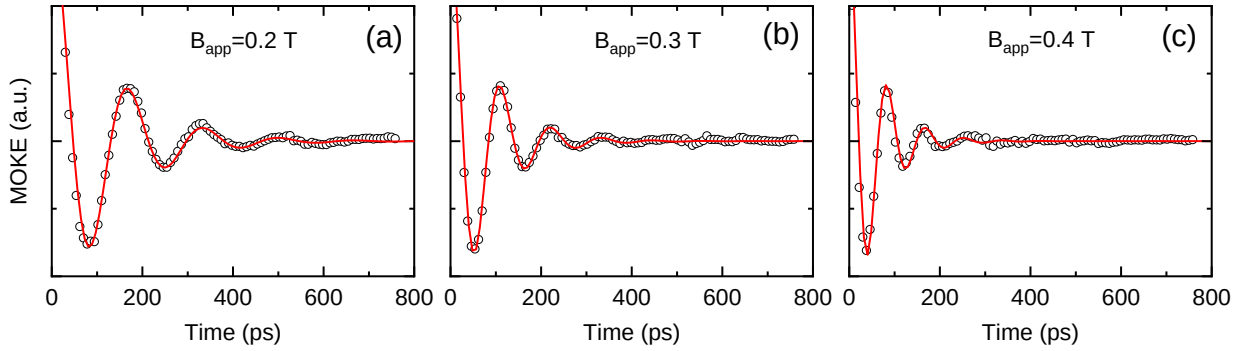

Figure A1. The B_{app} dependence on α_{eff}. The precessional motion in the $Gd_{24}Co_{76}$ alloys with B_{app} of (**a**) 0.2, (**b**) 0.3, and (**c**) 0.4 T along the *x*-direction. The black circles are obtained by subtracting the demagnetization background from the raw data of TRMOKE. The red lines are fittings by damped cosine function of $\cos(2\pi ft) \times \exp(-t/\tau)$. The fitted f values are 6.0, 8.9, and 11.8 GHz for (**a**–**c**), respectively. The fitted τ values are 120, 80, and 60 ps for (**a**–**c**), respectively.

References

1. Esho, S.; Fujiwara, S. Growth Induced Anisotropy in Sputtered GdCo Films. In *Magnetism and Magnetic Materials, Proceedings of the First Joint MMM-Intermag Conference, Pittsburgh, PA, USA, 15–18 June 1976*; AIP Publishing: College Park, MD, USA, 1976; Volume 34, pp. 331–333.
2. Taylor, R.; Gangulee, A. Magnetization and magnetic anisotropy in evaporated GdCo amorphous films. *J. Appl. Phys.* **1976**, *47*, 4666–4668. [CrossRef]
3. Mizoguchi, T.; Cargill, G., III. Magnetic anisotropy from dipolar interactions in amorphous ferrimagnetic alloys. *J. Appl. Phys.* **1979**, *50*, 3570–3582. [CrossRef]
4. Ostler, T.A.; Evans, R.F.L.; Chantrell, R.W.; Atxitia, U.; Chubykalo-Fesenko, O.; Radu, I.; Abrudan, R.; Radu, F.; Tsukamoto, A.; Itoh, A.; et al. Crystallographically amorphous ferrimagnetic alloys: Comparing a localized atomistic spin model with experiments. *Phys. Rev. B* **2011**, *84*, 024407. [CrossRef]
5. Stanciu, C.D.; Hansteen, F.; Kimel, A.V.; Kirilyuk, A.; Tsukamoto, A.; Itoh, A.; Rasing, T. All-optical magnetic recording with circularly polarized light. *Phys. Rev. Lett.* **2007**, *99*, 047601. [CrossRef]
6. Kirilyuk, A.; Kimel, A.V.; Rasing, T. Laser-induced magnetization dynamics and reversal in ferrimagnetic alloys. *Rep. Prog. Phys.* **2013**, *76*, 026501. [CrossRef] [PubMed]
7. Hansen, P.; Clausen, C.; Much, G.; Rosenkranz, M.; Witter, K. Magnetic and magneto-optical properties of rare-earth transition-metal alloys containing Gd, Tb, Fe, Co. *J. Appl. Phys.* **1989**, *66*, 756–767. [CrossRef]
8. Jiang, X.; Gao, L.; Sun, J.Z.; Parkin, S.S.P. Temperature dependence of current-induced magnetization switching in spin valves with a ferrimagnetic CoGd free layer. *Phys. Rev. Lett.* **2006**, *97*, 217202. [CrossRef]
9. Yang, Y.; Wilson, R.B.; Gorchon, J.; Lambert, C.-H.; Salahuddin, S.; Bokor, J. Ultrafast magnetization reversal by picosecond electrical pulses. *Sci. Adv.* **2017**, *3*, e1603117. [CrossRef]
10. Mishra, R.; Yu, J.; Qiu, X.; Motapothula, M.; Venkatesan, T.; Yang, H. Anomalous current-induced spin torques in ferrimagnets near compensation. *Phys. Rev. Lett.* **2017**, *118*, 167201. [CrossRef]
11. Cai, K.; Zhu, Z.; Lee, J.M.; Mishra, R.; Ren, L.; Pollard, S.D.; He, P.; Liang, G.; Teo, K.L.; Yang, H. Ultrafast and energy-efficient spin–orbit torque switching in compensated ferrimagnets. *Nat. Electron.* **2020**, *3*, 37–42. [CrossRef]

12. Sala, G.; Krizakova, V.; Grimaldi, E.; Lambert, C.-H.; Devolder, T.; Gambardella, P. Real-time Hall-effect detection of current-induced magnetization dynamics in ferrimagnets. *Nat. Commun.* **2021**, *12*, 1–9. [CrossRef] [PubMed]
13. Kim, K.-J.; Kim, S.K.; Hirata, Y.; Oh, S.-H.; Tono, T.; Kim, D.-H.; Okuno, T.; Ham, W.S.; Kim, S.; Go, G.; et al. Fast domain wall motion in the vicinity of the angular momentum compensation temperature of ferrimagnets. *Nat. Mater.* **2017**, *16*, 1187–1192. [CrossRef] [PubMed]
14. Siddiqui, S.A.; Han, J.; Finley, J.T.; Ross, C.A.; Liu, L. Current-induced domain wall motion in a compensated ferrimagnet. *Phys. Rev. Lett.* **2018**, *121*, 057701. [CrossRef] [PubMed]
15. Caretta, L.; Mann, M.; Büttner, F.; Ueda, K.; Pfau, B.; Günther, C.M.; Hessing, P.; Churikova, A.; Klose, C.; Schneider, M.; et al. Fast current-driven domain walls and small skyrmions in a compensated ferrimagnet. *Nat. Nanotechnol.* **2018**, *13*, 1154–1160. [CrossRef] [PubMed]
16. Ikeda, S.; Miura, K.T.; Yamamoto, H.; Mizunuma, K.; Gan, H.D.; Endo, M.; Kanai, S.; Hayakawa, J.; Matsukura, F.; Ohno, H. A perpendicular-anisotropy CoFeB–MgO magnetic tunnel junction. *Nat. Mater.* **2010**, *9*, 721–724. [CrossRef]
17. Ohmori, H.; Hatori, T.; Nakagawa, S. Perpendicular magnetic tunnel junction with tunneling magnetoresistance ratio of 64% using MgO (100) barrier layer prepared at room temperature. *J. Appl. Phys.* **2008**, *103*, 07A911. [CrossRef]
18. Yoshikawa, M. Tunnel magnetoresistance over 100% in MgO-based magnetic tunnel junction films with perpendicular magnetic L10-FePt electrodes. *IEEE Trans. Magn.* **2008**, *44*, 2573–2576. [CrossRef]
19. Rahman, M.T.; Liu, X.; Morisako, A. TiN underlayer and overlayer for TbFeCo perpendicular magnetic recording media. *J. Magn. Magn. Mater.* **2006**, *303*, e133–e136. [CrossRef]
20. Ceballos, A.; Pattabi, A.; El-Ghazaly, A.; Ruta, S.; Simon, C.P.; Evans, R.F.L.; Ostler, T.; Chantrell, R.W.; Kennedy, E.; Scott, M.; et al. Role of element-specific damping in ultrafast, helicity-independent, all-optical switching dynamics in amorphous (Gd,Tb)Co thin films. *Phys. Rev. B* **2021**, *103*, 024438. [CrossRef]
21. Sucksmith, W.; Thompson, J.E. The magnetic anisotropy of cobalt. *R. Soc. Lond. Ser. A Math. Phys. Sci.* **1954**, *225*, 362–375.
22. Okamoto, S.; Kikuchi, N.; Kitakami, O.; Miyazaki, T.; Shimada, Y.; Fukamichi, K. Chemical-order-dependent magnetic anisotropy and exchange stiffness constant of FePt (001) epitaxial films. *Phys. Rev. B* **2002**, *66*, 024413. [CrossRef]
23. Choi, G.-M.; Min, B.-C.; Shin, K.-H. $L1_0$ Ordering of FePtB Films on a Thin MgO Layer. *Appl. Phys. Express* **2011**, *4*, 023001. [CrossRef]
24. Nagaosa, N.; Sinova, J.; Onoda, S.; Macdonald, A.H.; Ong, N.P. Anomalous hall effect. *Rev. Mod. Phys.* **2010**, *82*, 1539–1592. [CrossRef]
25. Van Kampen, M.M.; Jozsa, C.C.; Kohlhepp, J.J.; LeClair, P.P.; Lagae, L.L.; De Jonge, W.J.M.; Koopmans, B.B. All-optical probe of coherent spin waves. *Phys. Rev. Lett.* **2002**, *88*, 227201. [CrossRef] [PubMed]
26. Binder, M.; Weber, A.; Mosendz, O.; Woltersdorf, G.; Izquierdo, M.; Neudecker, I.; Dahn, J.R.; Hatchard, T.D.; Thiele, J.-U.; Back, C.H.; et al. Magnetization dynamics of the ferrimagnet CoGd near the compensation of magnetization and angular momentum. *Phys. Rev. B* **2006**, *74*, 134404. [CrossRef]
27. Stanciu, C.D.; Kimel, A.V.; Hansteen, F.; Tsukamoto, A.; Itoh, A.; Kirilyuk, A.; Rasing, T. Ultrafast spin dynamics across compensation points in ferrimagnetic GdFeCo: The role of angular momentum compensation. *Phys. Rev. B.* **2006**, *73*, 220402. [CrossRef]
28. Kato, T.; Nakazawa, K.; Komiya, R.; Nishizawa, N.; Tsunashima, S.; Iwata, S. Compositional dependence of g-factor and damping constant of GdFeCo amorphous alloy films. *IEEE Trans. Magn.* **2008**, *44*, 3380–3383. [CrossRef]
29. Wangsness, R.K. Sublattice effects in magnetic resonance. *Phys. Rev.* **1953**, *91*, 1085–1091. [CrossRef]
30. Mizukami, S. Fast magnetization precession obsereved in $L1_0$-FePt epitaxial thin film. *Appl. Phys. Lett.* **2011**, *98*, 052501. [CrossRef]
31. Kim, D.-H.; Okuno, T.; Kim, S.K.; Oh, S.-H.; Nishimura, T.; Hirata, Y.; Futakawa, Y.; Yoshikawa, H.; Tsukamoto, A.; Tserkovnyak, Y.; et al. Low magnetic damping of ferrimagnetic GdFeCo alloys. *Phys. Rev. Lett.* **2019**, *122*, 127203. [CrossRef]